Photodetection Based on Ionic Liquid Gated Plasmonic Ag Nanoparticle/Graphene Nanohybrid Field Effect Transistors

Guowei Xu, Rongtao Lu, Jianwei Liu, Hsin-Ying Chiu,* Rongqing Hui, and Judy Z. Wu**

Graphene, an atomic layer of carbon atoms arranged in the honeycomb lattice,[1–3] has been one of the most attractive materials for optoelectronics because of its unique properties of remarkable charge mobility, high optical transmittance, chemical inertness and mechanical flexibility. Metal–graphene–metal Schottky photodetectors have been demonstrated at speeds over 40 GHz,[4] showing tunable photocurrents at the metal-graphene junction with various gate voltages. However, the light absorption of ~2.3% per layer of graphene[5] results in its relatively low photoresponsivity as compared to its conventional semiconductor counterparts employing typically absorber materials of tens to hundreds of nanometers in thickness. To address this issue, surface plasmon enhanced light absorption by various metallic nanostructures has been incorporated into graphene[6–8] and significant enhancement of photovoltage[8] at the metal-graphene junction and hence photocurrent[7,8] have been obtained. The additional benefit of the metallic plasmonic nanostructures is the wavelength selectivity accomplished through surface plasmon enhanced absorption at the plasmon resonance frequency.[7] Up to now, the best photoresponsivity obtained on metal-graphene-metal Schottky photodetectors is only about 0.4–0.5 mA/W at an operating wavelength of 514 nm,[7,8] which corresponds to external quantum efficiency of about 0.1%, and up to 6.1 mA/W at 1.55 μm.[9] Further exploration implementing plasmonic metal nanostructures has shown improved light absorption by up to 20 times and therefore enhanced photoresponsivity up to about 10 mA/W at wavelength of 514 nm,[8] which represents a substantial portion of the photoresponsivity upper limit of ~20 mA/W assuming 100% internal quantum efficiency for single-layer graphene. Considering the room for further improvement may be limited due to the theoretical upper limit, exploring different photodetection mechanisms using graphene becomes a necessity. One strategy employs nanostructured semiconductor photosensitizers/graphene hybrids, in which light absorption is achieved using nanoparticles,[10] nanorods,[11,12] or quantum dots.[13–16] While photoresponse with ultrahigh gain has been reported on these hybrid photodetectors, the instability of semiconducting nanostructures and the complicated ligand exchange process required present challenges for practical applications.[14,17] This motivates our work in exploring new mechanisms on graphene that do not deal with the above mentioned difficulties for photodetection.

The charge carrier density and hence electrical conductivity of graphene is highly susceptive to, and can be tuned by, gate electrostatic field E_G. The on/off ratio is over 5 in double-layer graphene field-effect transistors (FETs) at E_G ~3 MV/cm.[18] Higher gating efficiency, defined as the change of graphene channel conductivity per applied gate voltage V_G, can be obtained at larger gate capacitance, which can be achieved by using thinner high-κ dielectrics. A promising alternative is to use ionic liquid gate, which is highly efficient due to the formation of an electric double-layer with extremely small spacing on the order of 1 nm (the Debye length) near the graphene/ion liquid interface.[19] This renders a high gating efficiency on graphene.[20,21] A recent work on ionic liquid gated graphene FETs reveals the double-layer capacitance is as high as 9.2–21 μF/cm^2,[22,23] approximately 2–3 orders of magnitude higher than the back-gate capacitance using a layer of 90 nm SiO_2 (~38 nF/cm^2). In addition, the ionic liquid-gated graphene has shown to reach a high doping level of 5×10^{13}/cm^2,[24] mainly due to the ultrahigh breakdown field on the order of 1 MV/cm.[25]

The high-efficiency electrical gating of the ionic liquid may be correlated to an incident light through incorporation of plasmonic nanostructures on graphene FETs. It is known that an evanescent field can be generated near the nanostructure surface as a consequence of localized surface plasmonic resonance (LSPR) upon absorption of light with matching frequency to LSPR of the nanostructure.[26–29] Setting up a correlation between LSPR and the graphene FET gating may provide a highly efficient way to generate large photoconductivity and hence a new scheme for photodetection with high sensitivity.[30] An additional advantage of this scheme is the wavelength tunability determined by the LSPR frequency of the plasmonic nanostructure. By selecting plasmonic nanostructures of desired LSPR frequencies, photodetection at the targeted frequency range may be realized in a spectrum determined by the materials and geometric parameters of the plasmonic nanostructures.[31]

Herein, we report a novel graphene photodetector based on plasmonic Ag-NP/graphene nanohybrids FETs with an ionic liquid top gate. The fabrication process of the ionic liquid gated Ag-NP/graphene nanohybrid FETs is depicted schematically in **Figure 1**, consisting of six steps: CVD graphene sheet transferred onto substrate (Figure 1a), electrode deposition on graphene (Figure 1b), graphene FET fabrication (Figure 1c), Ag-NP self-assembly on graphene FET channel (Figure 1d), ionic liquid gate

Dr. G. W. Xu, Dr. R. T. Lu, Dr. J. W. Liu,
Prof. H.-Y. Chiu, Prof. J. Z. Wu
University of Kansas
Department of Physics and Astronomy
Lawrence, KS 66045, USA
E-mail: rtlu@ku.edu; chiu@ku.edu; jwu@ku.edu
Prof. R. Q. Hui
University of Kansas
Department of Electrical Engineering and Computer Science
Lawrence, KS 66045, USA

DOI: 10.1002/adom.201400077

ADVANCED OPTICAL MATERIALS
www.advopticalmat.de

www.MaterialsViews.com

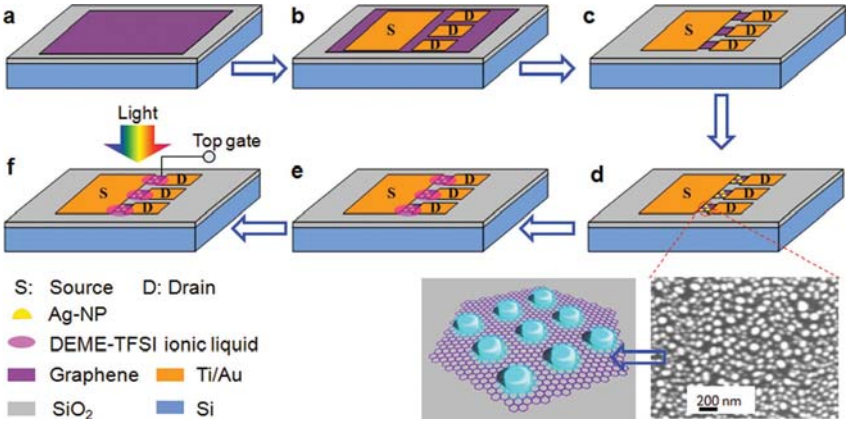

Figure 1. Ag-NP/graphene nanohybrid FETs fabrication process is depicted schematically following the steps of: (a) transfer of CVD-graphene onto SiO_2/Si substrate; (b) definition and deposition of Ti/Au electrodes using photolithography followed by electron beam evaporation; (c) definition of graphene FET channel using photolithography and reactive-ion etching; (d) Ag-NP fabrication on the graphene FET channel using metal film deposition through a shadow mask followed with thermal annealing; the blow-up view shows the SEM image of the AgNP surface on graphene and schematically the surface structure of the Ag-NPs/graphene nanohybrid; (e) casting ionic liquid on a graphene FET channel; and (f) attaching Pt wire to complete the top gate for photoresponse measurement.

deposition on graphene FET channel (Figure 1e) and top gate connection through a platinum wire immersed into the ionic liquid (Figure 1f). First, electrodes were formed by depositing 2 nm of titanium followed by 88 nm of gold in a high vacuum electron-beam evaporator on a sheet of centimeter-size single-layer CVD graphene transferred onto Si substrates capped with a thermal oxide layer of 90 nm in thickness (Figures 1a,b). Then the graphene sheet was patterned to an array of 4×9 FET devices using double-layer photolithography (LOR3B and S1813 photoresist) followed by reactive-ion etching (Figure 1c). In the FET array, the channel width is fixed at 20 μm while the channel length varies from 2 μm to 20 μm on different devices. Next, plasmonic Ag-NPs were obtained using thermally assisted self-assembly of Ag film deposited on graphene through a shadow mask on the FET channel (Figure 1d).[6] Thermal annealing in Ar (500 sccm)/H_2 (500 sccm) at 260 °C for 30 min was carried out to form Ag-NPs.[6] Transport measurements were made to characterize the back-gated graphene FETs before and after introduction of the plasmonic Ag-NPs. The surface structure of the graphene with Ag-NPs was indicated in the SEM image and schematic diagram as insets of Figure 1d, and the Ag-NPs has an average size of ~10–50 nm. The plasmonic Ag-NPs are hemispheric in shape as confirmed using atomic force microscopy. Finally, a droplet of ionic liquid was placed using a micropipette to cover the graphene channel with plasmonic Ag-NPs to form the top gate through a platinum wire, as shown in Figures 1e,f.

The Ag-NPs formed via thermally assisted self-assembly on graphene sheets obtained using chemical vapor deposition (CVD)[6,32] were used as the plasmonic nanostructures with the LSPR occurred at 420–470 nm for the Ag-NP diameters in the range of 10–50 nm using a similar self-assembly process we demonstrated recently.[6] In this experiment, the ionic liquid of *N,N*-diethyl-*N*-(2-methoxyethyl)-*N*-methylammonium *bis*-(trifluoromethylsulfonyl)-imide (DEME-TFSI) was employed as the gating material atop. DEME-TFSI was chosen owing to its large electrochemical window (±3 V), large capacitance and the minimal electrochemical reaction.[23] DEME-TFSI is transparent to allow incidence of light through and has been found in this work responsive to light-induced LSPR evanescent field via the electric double-layer deformation. At a microscopic scale, the molecular-based ions in ionic liquid may be deformed by the aforementioned plasmonic evanescent field via energy transfer (antenna effect), once the energy coupling is faster than the plasmon decay time of few tens of femto-seconds, resulting in electric field change through molecular geometry variations. Meanwhile, macroscopic geometric variation of the ionic liquid molecules may also occur considering the Ohmic damping (thermal effect when the energy coupling is not efficient) at the interfaces between Ag-NP/ionic liquid and neighboring regions by the evanescent field,[27] which may create temperature gradient in the proximity of the Ag-NPs and graphene surface, drive ion redistribution around the electric double layer. **Figure 2** depicts these two possible light-to-electrical field transducing mechanisms schematically in the double-gated

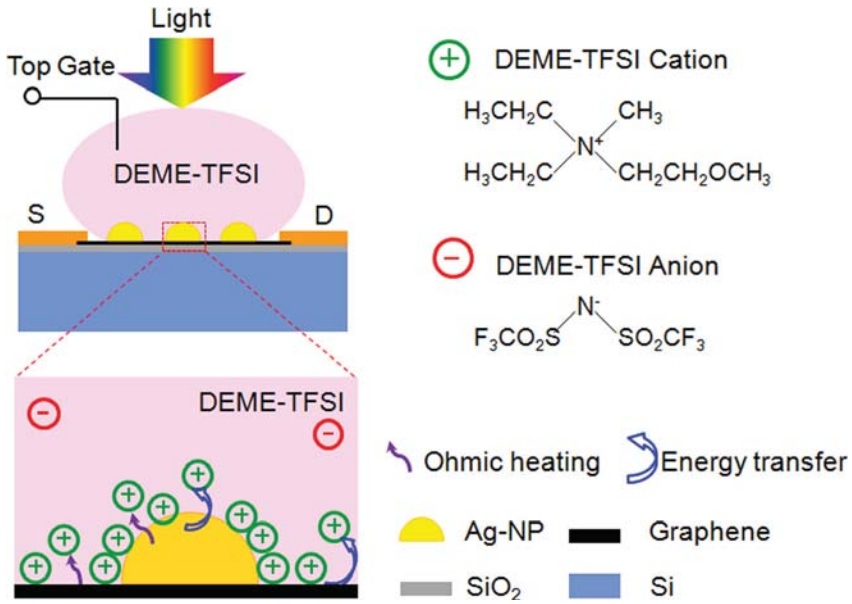

Figure 2. Schematics of Ag-NP/graphene nanohybrid FETs photodetectors with possible cation distribution changes around an Ag-NP through LSPR generated Ohmic heating or/and direct energy transfer.

plasmonic Ag NP/graphene nanohybrid FETs. The resulted perturbation from either or both effects to the top gate electric field upon light radiation and hence the interfacial capacitance and the quantum capacitance of graphene, will lead to change of the plasmonic Ag-NP/graphene nanohybrid FET channel conductivity as a photoresponse.

The source-drain current I_D was measured as the back-gate voltage V_{BG} on the graphene FETs on 90 nm silicon oxide using a Lakeshore probe station in the vacuum of 5×10^{-6} Torr and an Agilent B1500A semiconductor device analyzer. The same voltage scan rate was adopted in comparisons of the dark and illuminated source-drain currents The results obtained on a representative sample before and after the Ag-NP deposition are compared in **Figure 3**a. The Dirac point (or neutrality point) voltage V_{Dirac} of the CVD graphene (black) used in this experiment is typically on the positive side indicative of the *p*-type doping. Upon deposition of Ag-NPs, the V_{Dirac} shifts to the negative side (red), due to *n*-type doping through the Ag/graphene interface. This is consistent with the previous reports and is attributed to electron doping from Ag to graphene.[33] The specific value of V_{Dirac} on Ag-NP/graphene nanohybrids depends on the morphology of the Ag-NPs and their interface with graphene. Typically, a larger shift of V_{Dirac} was observed for the higher coverage of Ag-NPs on graphene and better interfaces between them. In addition to the V_{Dirac} shift at Ag-NP deposition, the minimum conductance of graphene at the Dirac point increases by approximately a factor of 2–4, which is consistent to our previous observation on Ag-NP/graphene nanohybrid transparent conductors possibly due to a parallel path for charge transport provided by Ag-NPs to graphene.[6]

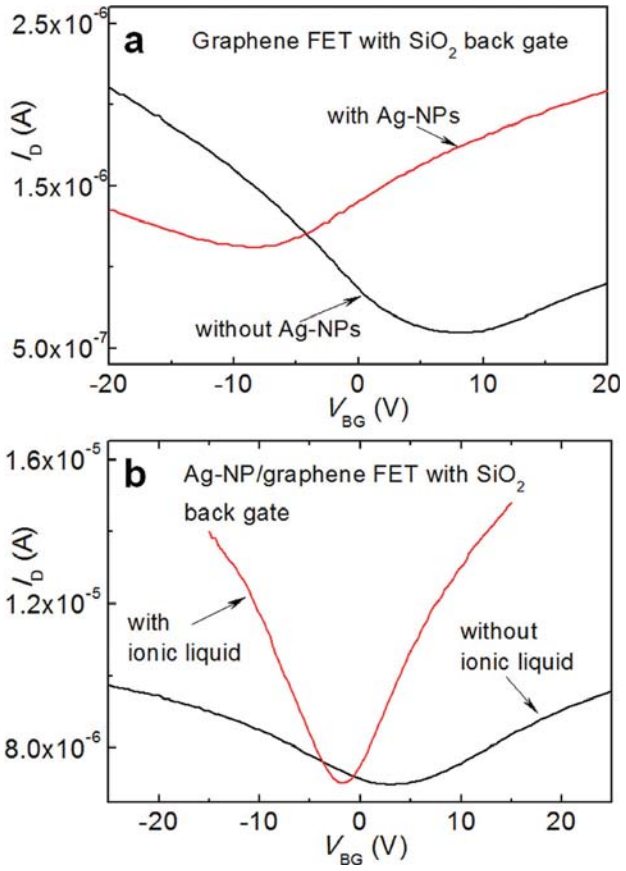

Figure 3. The I_D-V_{BG} curves for: (a) a representative back-gated graphene FET on 90 nm thick SiO_2 with (red) and without (black) Ag-NPs; and (b) a representative back-gated Ag-NP/graphene nanohybrid FET before (black) and after (red) application of ionic liquid on the top of the FET channel while the platinum wire used for top gate measurement was not attached. V_{SD} = 10 mV.

After application of the DEME-TFSI ionic liquid on top of the plasmonic Ag-NP/graphene nanohybrid FET channels, the gate electric field E_G may be applied either from the SiO_2 bottom gate or from the ionic liquid top gate. To quantify the floating gate effect of the ionic liquid on the transport properties of plasmonic Ag-NP/graphene nanohybrid FETs, the $I_D - V_{BG}$ curves were compared using the back-gate geometry before and after the application of the ionic liquid on top of the FET channel. The obtained I_D–V_{BG} curves on a representative sample are compared in Figure 3b at V_{SD} = 10 mV. It is clearly seen that the Dirac point is negatively shifted (observed on the majority of more than 20 samples studied) after the ionic liquid application but at zero applied gate voltage V_{TG}. In addition, the slope of the I_D–V_{BG} curve becomes considerably steeper on both electron and hole branches as a consequence of the additional capacitive gating effect through the ionic liquid/graphene interface. This is not surprising considering the large interfacial capacitance of the ionic liquid DEME-TFSI in the range of 9.2–21 μF/cm^2,[22,23] and therefore a much higher gating efficiency as compared to the case of the dielectric gates. Consequently, much smaller V_{TG} is needed to achieve the same gating efficiency as compared to the V_{BG} in the double-gate graphene FETs studied in this work. Interestingly, the minimum conductance of the graphene FET channel remains the same, indicating the application of ionic liquid does not introduce significant charge scattering at graphene-ionic liquid interface.

The photoresponse of the ionic liquid top-gated plasmonic Ag-NP/graphene nanohybrid FETs was characterized first using white light with power intensity of about 100 mW/cm^2. In order to elucidate the mechanism of the photoresponse, three other FET configurations obtained at different steps in the FET fabrication process shown in Figure 1, were also tested under the same experimental condition. They include back-gated graphene FET (after the fabrication step of Figure 1c), back-gated plasmonic Ag-NP/graphene nanohybrid FET (after the fabrication step of Figure 1d), and ionic liquid top-gated graphene FET (ionic liquid applied directly on graphene after the fabrication step of Figure 1c). The measurements under light illumination were taken at 1 minute after light was turned on. The $I_D - V_G$ (back gate voltage V_{BG} for the first two cases and top gate voltage V_{TG} for the third one) curves taken on these three types of devices in dark and illuminated conditions are shown in **Figures 4**a–c, and none of them displayed any measureable photoresponse. (Please be noted that the data were collected from different samples due to the different device structure and configuration, thus some parameters such as Dirac point positions and minimum conductivities are slightly different from sample to sample.) In contrast, a clear shift of the $I_D - V_{TG}$ curve can be observed in Figure 4d on the ionic liquid top-gated plasmonic Ag-NP/graphene nanohybrid FETs (device illustrated in Figure 1f) in response to light on (red curve). At V_{TG} = 0, for example, the photoresponse is $\Delta I_D = I_{D,Illuminated} - I_{D,Dark} \approx 56$ nA,

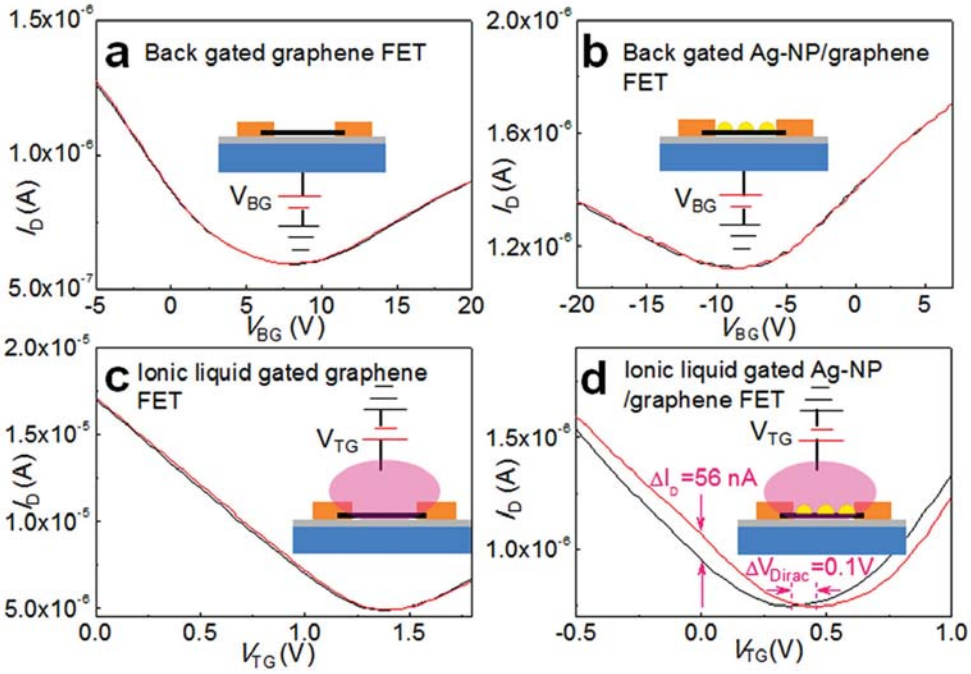

Figure 4. I_D-V_G curve measured in dark (black) and with white light illumination (red) for four kinds of FET devices: (a) back-gated graphene FET; (b) back-gated Ag-NP/graphene nanohybrid FET; (c) ionic-liquid top-gated graphene FET; (d) ionic-liquid top-gated Ag-NP/graphene nanohybrid FET. The insets show the corresponding device geometries. The intensity of the white light was 100 mW/cm^2.

which is a representative value in the range of 30–60 nA observed inmore than 20 samples in this work with Ag-NPs generated under the same condition.

The light-induced Dirac point shift may be directly correlated to the change of the specific interfacial capacitance (capacitance per unit area) $C_{IC} = \frac{\varepsilon\varepsilon_0}{t}$, where ε is the dielectric constant of the ionic liquid and t is the separation of accumulated ions from graphene surface in the case of using ionic liquid as top gate dielectrics. From the definition of interfacial capacitance, only t is responsible for its change. So the Dirac point shift of the plasmonic Ag-NP/graphene nanohybrid FETs upon illumination is very likely to be attributed to the change of separation of accumulated ions from graphene as well as quantum capacitance. In other words, this photoresponse with Dirac point shift is caused by the deformation or modified distribution of accumulated ions at the graphene surface. In this circumstance, the quantum capacitance of graphene C_{QC} is taken into account since C_{IC} is comparable to C_{QC} and they are considered to gate the graphene in series. Thus the total specific gate capacitance C may be derived from:

$$\frac{1}{C} = \frac{1}{C_{IC}} = \frac{1}{C_{QC}} \tag{1}$$

In graphene, the specific quantum capacitance is defined as $C_{QC} = \frac{e^2}{\pi\hbar v_F}\sqrt{\pi n}$, where the Fermi velocity v_F is about 1/300 of the speed of light and n is the 2D charge carrier density in graphene. The combined effect of the C_{QC} and C_{IC} on the gate electrical field can be described using the equation below,[24] in which the first term on the right side of the Equation (2) is for C_{QC} and the second term is for C_{IC}:

$$V_{TG} - V_{Dirac} = \frac{\hbar v_F \sqrt{\pi n}}{e} + \frac{ne}{C_{IC}} \tag{2}$$

Using C_{IC} = 9.2 μF/cm^2 (the lower limit of the C_{IC} for its maximum contribution in Equation (2),[23] for example, we can obtain

$$V_{TG} - V_{Dirac} = 1.16\times10^{-7}\sqrt{n} + 0.173\times10^{-13}n \tag{3}$$

Therefore, from Equation (3), the contribution from interfacial capacitance cannot be neglected when the carrier density of graphene is on the order of 10^{12}/cm^2 or higher. This means that a change in C_{IC} due to the change in effective t induced by ions distribution variation may result in considerable shift of the Dirac point of graphene. Thus, coupling light illumination via LSPR on Ag-NPs deposited directly on the graphene surface may provide an efficient way to modify the distribution of ions in the ionic liquid on the surface of graphene and to transduce light to photoconductivity as demonstrated in this work.

The interfacial capacitance of ionic liquid as well as the quantum capacitance of graphene was varied upon light illumination via the LSPR field from the plasmonic Ag-NPs, resulting in photoresponse through photoconductivity. At V_{TG} = 0, the ΔI_D upon illumination is around 56 nA for the sample shown in Figure 4d, which results in photoresponsivity of 140 mA/W, corresponding to photoconductivity of 14 S/W based on the size of the graphene device (20 × 20 μm^2):

$$Photoresponsivity = \frac{\Delta I_D}{Incident-light-power} = \frac{56\,nA}{100\,mW/cm^2 \times (20\,\mu m)^2} = 140\,mA/W \quad (4)$$

$$Photoconductivity = \frac{140\,mA/W}{10\,mV} = 14\,S/W \quad (5)$$

This photoresponsivity is over an order of magnitude higher than the previously reported value on metal–graphene–metal Schottky photodetectors either with or without plasmonic nanostructures.[7,8] In particular, this was obtained at almost zero gate voltage, which is favorable in terms of low energy consumption and device simplification.

To confirm this photoresponse is originated from the LSPR on the Ag-NPs, single wavelength laser beams with various wavelengths were used to repeat the photoresponse measurement under the same conditions. Prior to the photoresponse measurement, the LSPR wavelength of graphene with Ag-NPs immersed in ionic liquid was determined by both simulation (**Figure 5**a) and direct optical transmittance measurement (Figure 5b). In the former, a *FULLWAVE* finite-difference time-domain (FDTD) simulation package from the R-Soft Inc. was employed. The Ag-NP structure was simulated as Ag disk for simplicity of calculation. As depicted schematically in the inset of Figure 5a, an ideal Ag disk with a thickness of 10 nm and a diameter of 20 nm was placed on the graphene on the front surface of a silica substrate representing the 90-nm-thick oxide layer on silicon. A plane lightwave was normally launched with a single polarized electrical field E_x. The simulation area was 60 nm × 60 nm in the horizontal dimension, and 50 nm in the direction normal to the interface with the Ag disk in the center. Perfectly matched layer conduction was used as the boundary of simulation window which absorbs the energy without inducing reflections. Only one Ag disk was included in the simulation area to reduce the simulation time. As a consequence the effect of interference between different Ag-NPs was not included. Optical power flow was integrated over a box surrounding the Ag disk using the Q-calculation function of the simulation package, and the calculated Q value is proportional to the absorption cross section area of the Ag-NP. Drude model was applied for the dielectric function of Ag, and a complex refractive index $n_g = 2.4 + i \cdot 1$ was used for graphene.[34] Figure 5a shows the calculated Q-values as the function of wavelength for an Ag disk on graphene/silica substrate with (open squares) and without (open circles) ionic liquid immersing the Ag disk. The calculated LSPR resonance wavelength is approximately 460 nm for the plasmonic Ag-NP/graphene nanohybrids without ionic liquid, while it red shifts to about 520 nm together with enhanced plasmonic resonance amplitude when the ionic liquid is applied. This is not surprising since the replacement of the semi-infinite free-space by the ionic liquid will increase the average material refractive index surrounding the Ag disk, leading to the red shift of the plasmonic resonance wavelength and enhancement of the resonance amplitude.

Direct measurement of optical transmittance of plasmonic Ag-NP/graphene nanohybrids reveals qualitatively consistent

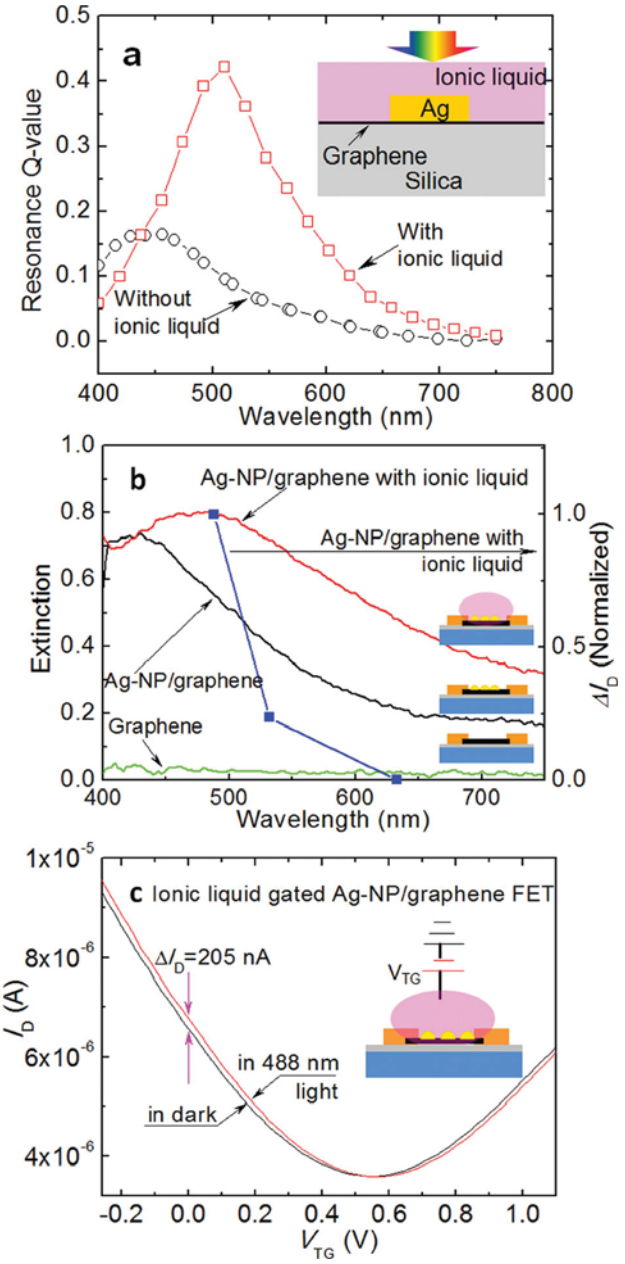

Figure 5. Wavelength dependence of photoresponse. (a) FDTD simulated resonance Q-value as function of wavelength for ionic liquid covered Ag-NP/graphene. The Ag disk has 10 nm in thickness and 20 nm in diameter. (b) Measured transmittance curves of graphene, Ag-NP/graphene nanohybrid covered with or without ionic liquid (left coordinate). The ΔI_D values measured at $V_{TG} = 0$ on ionic-liquid gated Ag-NP/graphene nanohybrid FETs at light source wavelengths of 488 nm, 532 nm and 633 nm (right coordinate) are overlaid on the transmittance curve of ionic-liquid covered Ag-NP/graphene nanohybrid. (c) Representative I_D–V_{TG} curves of an ionic liquid gated Ag-NP/graphene FET in dark and 488 nm illumination (~102 mW/cm^2), V_{SD} = 10 mV.

results as shown in Figure 5b. The optical transmittance was measured using a Horiba iHR550 spectrometer and a Labsphere Integrating Sphere. The CVD graphene on glass substrate (black) shows a wideband absorption of 2–3% over the visible wavelengths as expected. The LSPR wavelength

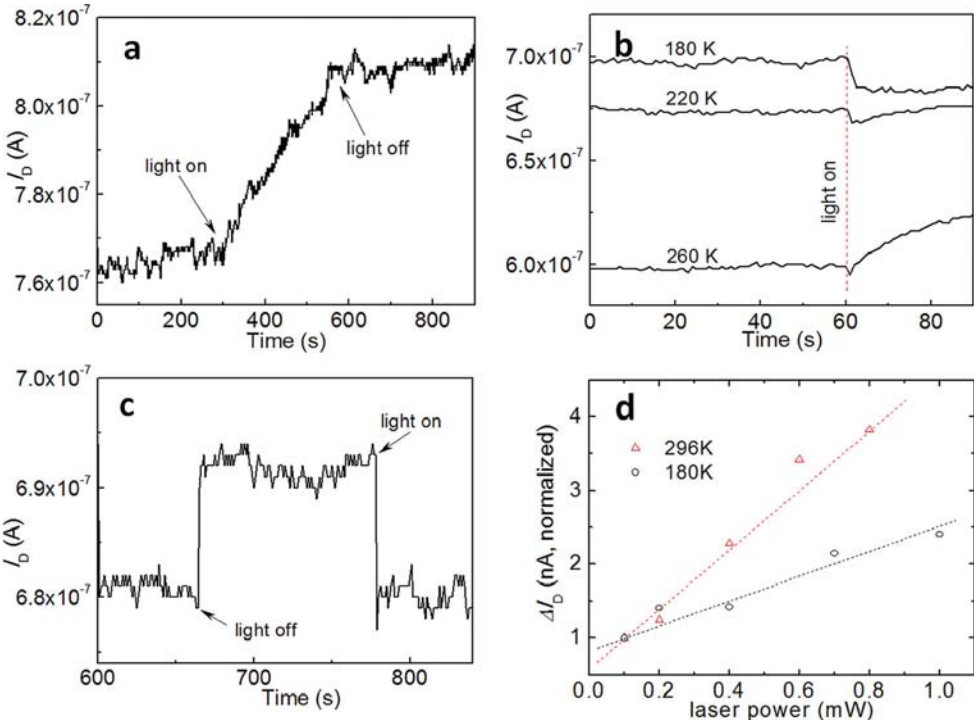

Figure 6. Dynamic photoresponses upon incident white light of 100 mW/cm^2 measured on the ionic liquid gated Ag-NP/graphene nanohybrid FETs at different temperatures at: (a) room temperature; (b) three cryogenic temperatures near and above the ionic liquid glass transition point. The dashed line shows the time the incident light was turned on. (c) Dynamic photoresponse to the modulated white light at 180K. V_{TG} = 0 V and V_{SD} = 5 mV for (a)-(c). (d) The absolute value of the observed ΔI_D (at zero gate bias) in Ag-NP/graphene FET versus incident power of 488 nm laser at 296 K and 180 K. The absolute values of the observed ΔI_D are compared since the response at 180 K has opposite sign to that at 296 K, and the two dashed lines are plotted to show the trends of the variations.

measured on the Ag-NP/graphene nanohybrid samples before application of the ionic liquid is around 430 nm, suggested by the peak in the extinction curve (red) in Figure 5b. Note that the calculated resonance wavelength is slightly (~30 nm) longer than the measured ones. This minor discrepency could be caused by the uncertainty of shapes and sizes of the Ag-NPs. With application of the ionic liquid DEME-TFSI, whose refractive index is around 1.4–1.5,[35] the LSPR wavelength red shifts to around 480 nm, which is attributed to the increased refractive index of the medium surrounding the Ag-NPs[36] and the trend agrees with the FDTD simulation based on this consideration. The slightly smaller red-shift of 50 nm, as compared to 60 nm predicted by the simulation, may be due to the imperfect interface configuration between the ionic liquid and the Ag-NP/graphene nanohybrid. Considering the LSPR wavelength range of the Ag-NP/graphene nanohybrids in ionic liquid, visible lasers of 488 nm, 532 nm and 633 nm wavelengths as well as infrared (IR) light source (wavelength ~ 1000–1300 nm) were used for optical illumination at the same intensity. The measured photoresponse ΔI_D (black squares, normalized to the response current value at 488 nm) at V_{TG} = 0 was superimposed on the transmittance-wavelength curve in Figure 5b. Among the photoresponse measured at 488 nm, 532 nm, 633 nm and 1000–1300 nm, the highest photoresponse was observed at the 488 nm laser illumination which is almost right on the LSPR wavelength of the Ag-NP/graphene nanohybrids. The photoresponse decreases dramatically with increasing light wavelength. For example, the photoresponse at the 532 nm laser illumination decreased to approximately 25% of that at 488 nm (Figure 5b) and it was barely measurable at 633 nm (Figure 5b) or near-IR illumination (not shown). This strong wavelength selectivity of the photoresponse, in particular, with the dramatically stronger photoresponse observed at the LSPR wavelength of the Ag-NP/graphene nanohybrids in ionic liquid, confirms the role of the plasmonic Ag-NPs in terms of enhancing light trapping at the LSPR wavelength and transducing the light to photoconductivity via interface capacitance change.

Figure 5c shows the representative I_D-V_{TG} curves of an ionic liquid top-gated Ag-NP/graphene FET (the same device configuration as in Figure 4d) under dark and 488 nm laser with incident intensity of 102 mW/cm^2, and V_{SD} was kept at 10 mV. Upon 488 nm laser illumination, the Dirac point shifts to the right side in a similar way to that observed in the white light (Figure 4d), inducing a photocurrent change of ΔI_D ~ 205 nA at V_{TG} = 0V. Considering the dimension ~ 22 μm ×13 μm for this sample, the obtained responsivity of about 350 mA/W is significantly greater than that observed in white light (140 mA/W) of comparable light intensity and experimental setting. This result is anticipated and further confirms the dominant role of the LSPR effect in the ionic liquid gated plasmonic Ag-NP/Graphene nanohybrid FET photodetectors reported in this work.

The dynamic photoresponse was measured and the result at room temperature is shown in **Figure 6**a at zero gate voltage and V_{SD} = 5 mV. The smaller source-drain voltage was used to decrease the ion motion along the source-drain direction. After light was turned on, a significant increase of I_D of approximately

40 nA can be observed at ~ 600 s. The slow photoresponse may be attributed to the slow motion of ions in the ionic liquid,[37] which indicates that the photoresponse observed at room temperature is primarily caused by the movement of accumulated ions at the graphene surface. This suggests the macroscopic geometric variation of the ionic liquid molecules distribution may be a dominant reason due to the Ohmic heating near Ag-NPs by the LSPR evanescent field,[27] as we discussed earlier on Figure 2. Once the light was off, I_D current relaxed to its starting point in a period of over an hour under no applied electric field while the application of AC field or DC with changing polarity can reset the sample back to the starting point instantaneously. The macroscopic ion motion may be much reduced by cooling the sample to near or below the glass transition temperature ~ 182 K[19] of the DEME-TFSI as the ionic transport decreases monotonically with decreasing temperatures.[38] To shed some lights on this, the dynamic photoresponse of the same plasmonic Ag-NP/graphene nanohybrid FET sample as shown in Figure 4d was measured at different temperatures in the range of 180–350 K and the data for 180 K, 220 K and 260 K at zero gate voltage are compared in Figure 6b. Interestingly, the two lower temperature curves have an opposite photoresponse to that of the higher temperature one (i.e., Dirac point shifts to left as opposed to right at room temperature) . In addition, the former is much faster than the latter. While the microscopic mechanism is still under investigation, we speculate this faster photoresponse may be attributed to the direct energy transfer from LSPR excited on the Ag-NPs to ion molecules in the DEME-TFSI, such as the oxygen-containing functional groups. The follow-up relaxation may result in a charge transfer in a similar way to photovoltaic process and a perturbation to the local electric field on graphene. At the temperatures above the DEME-TFSI glass transition point, our result suggests the effects of the photoresponse due to LSPR energy transfer and Ohmic heating co-exist. With reducing temperatures to near the ionic liquid glass transition point, the LSPR Ohmic heating driven motion of the ionic liquid molecules is effectively suppressed due to the reduced ionic transport, allowing observation of the faster and smaller photoresponse dominated possibly by the direct energy transfer. In the temperature range from 180 K to 220 K, the amplitude of the total negative photoresponse decreases with increasing temperature, due to cancellation of the two types of the photoresponse. At temperatures much above the ionic liquid glass transition point, the LSPR Ohmic heating-caused positive photoresponse dominates. Nevertheless, a small dip (negative, microscopic) in the photoresponse remains visible even at 260 K immediately after the light was turned on, followed with a slowly increasing positive photoresponse of macroscopic origin.

The photoresponse of the LSPR energy-transfer origin responds to both light "On" and "Off" promptly as shown in Figure 6c at 180 K. The response time of smaller than 20 milliseconds is estimated based on the prompt photoresponse upon light modulation using 20 Hz chopper and the measured photoresponse has a similar square-wave shape of the incident light. While higher frequency measurement was not available due to the instrument limitation of the semiconductor analyzer, the obtained result at lower frequencies indicates a clearly different origin in the observed photoresponse at 180 K as opposed to that at room temperature on the ionic liquid gated plasmonic Ag-NP/graphene nanohybrid FETs.

It should be noted that both of the LSPR Ohmic heating and energy transfer induced photoresponse share the same wavelength dependence, indicative of their correlations with the LSPR of the plasmonic Ag-NP/graphene nanohybrid. As shown in Figure 6d, a more or less linear dependence of the photoresponse ΔI_D on the 488 nm light intensity, measured at 180 K and 296 K respectively, seems consistent with this argument. It should be pointed out that this figure is comparing the absolute values of the observed ΔI_D, since the response at 180 K has opposite sign to that at 296 K. In both cases, the photoresponse increases monotonically with the light intensity while the slope for the former is smaller than that of the latter, which may be attributed to the different coupling efficiencies of LSPR to E_G through the two mechanisms.

In summary, a new photodetection scheme has been demonstrated on ionic liquid gated plasmonic Ag-NP/graphene nanohybrid FETs, which takes the full advantages of the LSPR-based light trapping by the plasmonic nanostructures integrated with the high gating efficiency of the ionic liquid on graphene FET channel conductivity. High responsivity and wavelength tunability have been demonstrated. At room temperature, the obtained photoresponsivity of ~350 mA/W upon incident light with wavelength close to the LSPR wavelength on these devices is more than an order of magnitude higher than the best reported on the metal-graphene-metal Schottky photodiodes with plasmonic nanostructures. At lower temperatures, a photoresponse of reversed polarity and shorter response time was observed. Two different coupling mechanisms of the LSPR-to-E_G have been identified in these ionic liquid gated plasmonic Ag-NP/graphene nanohybrid FETs. The slower coupling attributed to the LSPR Ohmic heating dominates the photoresponse near room temperature while the faster one attributed to the direct LSPR energy transfer plays the primary role in photoresponse at lower temperatures near the ionic liquid glass transition temperature.

Acknowledgments

The authors acknowledge support in part by ARO contract No. ARO-W911NF-12–1–0412, and NSF contracts Nos. NSF-DMR-1105986 and NSF EPSCoR-0903806, and matching support from the State of Kansas through Kansas Technology Enterprise Corporation. H.-Y. C thank J. Wei for providing liquid electrolyte and H.-C. Chien for helpful discussions.

Received: February 17, 2014
Revised: April 11, 2014
Published online: May 30, 2014

[1] J. K. Wassei, R. B. Kaner, *Mater. Today* **2010**, *13*, 52.
[2] F. Bonaccorso, Z. Sun, T. Hasan, A. C. Ferrari, *Nat. Photonics* **2010**, *4*, 611.
[3] K. S. Novoselov, A. K. Geim, S. V. Morozov, D. Jiang, Y. Zhang, S. V. Dubonos, I. V. Grigorieva, A. A. Firsov, *Science* **2004**, *306*, 666.
[4] F. N. Xia, T. Mueller, Y. M. Lin, A. Valdes-Garcia, P. Avouris, *Nat. Nanotechnol.* **2009**, *4*, 839.
[5] R. R. Nair, P. Blake, A. N. Grigorenko, K. S. Novoselov, T. J. Booth, T. Stauber, N. M. R. Peres, A. K. Geim, *Science* **2008**, *320*, 1308.

[6] G. W. Xu, J. W. Liu, Q. Wang, R. Q. Hui, Z. J. Chen, V. A. Maroni, J. Wu, *Adv. Mater.* **2012**, *24*, Op71.
[7] Y. Liu, R. Cheng, L. Liao, H. L. Zhou, J. W. Bai, G. Liu, L. X. Liu, Y. Huang, X. F. Duan, *Nature Commun.* **2011**, *2*, 579.
[8] T. J. Echtermeyer, L. Britnell, P. K. Jasnos, A. Lombardo, R. V. Gorbachev, A. N. Grigorenko, A. K. Geim, A. C. Ferrari, K. S. Novoselov, *Nature Commun.* **2011**, *2*, 458.
[9] T. Mueller, F. N. A. Xia, P. Avouris, *Nat. Photonics* **2010**, *4*, 297.
[10] K. H. Zheng, F. B. Meng, L. Jiang, Q. Y. Yan, H. H. Hng, X. D. Chen, *Small* **2013**, *9*, 2076.
[11] J. Liu, R. Lu, G. Xu, J. Wu, P. Thapa, D. Moore, *Adv. Funct. Mater.* **2013**, *23*, 4941.
[12] H. Chang, Z. Sun, K. Y.-F. Ho, X. Tao, F. Yan, W.-M. Kwok, Z. Zheng, *Nanoscale* **2011**, *3*, 258.
[13] Z. H. Sun, Z. K. Liu, J. H. Li, G. A. Tai, S. P. Lau, F. Yan, *Adv. Mater.* **2012**, *24*, 5878.
[14] R. Ihly, J. Tolentino, Y. Liu, M. Gibbs, M. Law, *ACS Nano* **2011**, *5*, 8175.
[15] G. Konstantatos, M. Badioli, L. Gaudreau, J. Osmond, M. Bernechea, F. P. G. de Arquer, F. Gatti, F. H. L. Koppens, *Nat. Nanotechnol.* **2012**, *7*, 363.
[16] D. Y. Zhang, L. Gan, Y. Cao, Q. Wang, L. M. Qi, X. F. Guo, *Adv. Mater.* **2012**, *24*, 2715.
[17] G. Konstantatos, L. Levina, A. Fischer, E. H. Sargent, *Nano Lett.* **2008**, *8*, 1446.
[18] F. Xia, D. B. Farmer, Y. M. Lin, P. Avouris, *Nano Lett.* **2010**, *10*, 715.
[19] T. Sato, G. Masuda, K. Takagi, *Electrochim. Acta* **2004**, *49*, 3603.
[20] H. G. O. Sandberg, T. G. Backlund, R. Osterbacka, H. Stubb, *Adv. Mater.* **2004**, *16*, 1112.
[21] H. T. Yuan, H. Shimotani, A. Tsukazaki, A. Ohtomo, M. Kawasaki, Y. Iwasa, *Adv. Funct. Mater.* **2009**, *19*, 1046.
[22] J. L. Xia, F. Chen, J. H. Li, N. J. Tao, *Nat. Nanotechnol.* **2009**, *4*, 505.
[23] J. T. Ye, S. Inoue, K. Kobayashi, Y. Kasahara, H. T. Yuan, H. Shimotani, Y. Iwasa, *Nat. Mater.* **2010**, *9*, 125.
[24] A. Das, S. Pisana, B. Chakraborty, S. Piscanec, S. K. Saha, U. V. Waghmare, K. S. Novoselov, H. R. Krishnamurthy, A. K. Geim, A. C. Ferrari, A. K. Sood, *Nat. Nanotechnol.* **2008**, *3*, 210.
[25] R. Kotz, M. Carlen, *Electrochim. Acta* **2000**, *45*, 2483.
[26] S. Y. Yin, Q. L. Deng, X. G. Luo, C. L. Du, Y. D. Zhang, *J. Appl. Phys.* **2008**, *104*, 024308.
[27] H. A. Atwater, A. Polman, *Nat. Mater.* **2010**, *9*, 205.
[28] K. R. Catchpole, A. Polman, *Opt. Express* **2008**, *16*, 21793.
[29] K. R. Catchpole, A. Polman, *Appl. Phys. Lett.* **2008**, *93*, 191113.
[30] Z. Y. Fang, Y. M. Wang, Z. Liu, A. Schlather, P. M. Ajayan, F. H. L. Koppens, P. Nordlander, N. J. Halas, *ACS Nano* **2012**, *6*, 10222.
[31] J. M. Luther, P. K. Jain, T. Ewers, A. P. Alivisatos, *Nat. Mater.* **2011**, *10*, 361.
[32] J. Liu, G. Xu, C. Rochford, R. Lu, J. Wu, C. M. Edwards, C. L. Berrie, Z. Chen, V. A. Maroni, *Appl. Phys. Lett.* **2011**, *99*, 023111.
[33] G. Giovannetti, P. A. Khomyakov, G. Brocks, V. M. Karpan, J. van den Brink, P. J. Kelly, *Phys. Rev. Lett.* **2008**, *101*, 026803.
[34] X. F. Wang, Y. P. Chen, D. D. Nolte, *Opt. Express* **2008**, *16*, 22105.
[35] P. Bonhote, A. P. Dias, N. Papageorgiou, K. Kalyanasundaram, M. Gratzel, *Inorg. Chem.* **1996**, *35*, 1168.
[36] G. Xu, M. Tazawa, P. Jin, S. Nakao, K. Yoshimura, *Appl. Phys. Lett.* **2003**, *82*, 3811.
[37] T. Sato, T. Morinaga, S. Marukane, T. Narutomi, T. Igarashi, Y. Kawano, K. J. Ohno, T. Fukuda, Y. Tsujii, *Adv. Mater.* **2011**, *23*, 4868.
[38] T. Fujimoto, K. Awaga, *Phys. Chem. Chem. Phys.* **2013**, *15*, 8983.